1540160 Using Microseismicity to Understand Subsurface Fracture Systems and Increase the Effectiveness of Completions: Eagle Ford Shale, TX

John P. Detring[1] and Sherilyn Williams-Stroud[2]

1. Analysis, MicroSeismic Inc., Denver, CO, United States. 2. Worldwide Exploration | Rock Sciences Group, Occidental Oil & Gas Corp., Houston, TX, United States.

Summary

Existing natural fractures often have a significant impact on both stimulation and production of oil and gas wells. Effective exploitation of unconventional reservoirs requires the understanding of the local tectonic history and the present day stress regime. Signal strength, high quality reflection seismic, microseismic imaging, and moderate structural complexity of the liquids-rich gas and tight oil Eagle Ford shale makes it an ideal place to study hydraulic fracturing in tight rocks. Microseismic monitoring results showed clear structural trends relating to reactivation of existing faults and fractures, and rock failure mechanisms determined through source mechanism inversion of events. These results provided critical information to the operator for optimizing the hydraulic fracture design.

Microseismic data collected using a surface array allowed the full geometry of the result to be viewed with no directional bias. The geometry of the microseismicity trends related to fracturing developed during the stimulation treatment was representative of the true geometry of the structure. The large aperture and wide azimuth of the monitoring array facilitated the determination of source mechanisms from every event detected, which provided full coverage of the focal sphere of each source mechanism. The events identified two different source mechanisms, indicating a different failure mechanism for fractures than for reactivated faults.

Microseismicity with a NE-SW orientation are interpreted to be related to either induced or reactivated fractures. Microseismicity also formed trends that are contiguous across more than one wellbore in an ENE-WSW direction. These trends are interpreted to have formed as a result of fault reactivation. Source mechanisms from fracturing parallel to S_{Hmax} have failure planes that strike NE-SW with normal dip-slip failure on steeply-dipping planes. Those from fault reactivation have strike-slip failure on ENE-WSW striking failure planes. The orientations of the fracturing-related trends are parallel to extensional Gulf of Mexico growth faulting. The microseismicity trends associated with fault reactivation form at an angle of approximately 25° to the fracturing trends.

Microseismicity trends associated with faults are used to project where faults will intersect adjacent wells. Identification of these faults in the reservoir via microseismic mapping allow operators to modify their treatment parameters and stage spacing in order to avoid geologic hazards. The operator combines the treatment pump parameters for the wells with the additional structural understanding gained from the analysis of fracture trends and source mechanisms to identify zones that should be avoided in subsequent treatments. In addition, the mapped microseismicity provides critical information that was used to modify well spacing for subsequent wells, thereby optimizing the completion plan and dramatically cutting costs.

Introduction

The Eagle Ford Shale is ideal for microseismic mapping. The microseismicity has a high signal to noise ratio, resulting in high accuracy of event locations and source mechanism inversions. The same low attenuation and high signal quality imaging factors in this basin that lead to high quality reflection seismic data quality also allow high quality microseismic imaging.

The coastal plain of south Texas is characterized by NNE-SSW to ENE-WSW striking, steeply-dipping, growth faults. Figure 1 shows the structural geology of south Texas. In addition to potential reactivation of these faults by the hydraulic fracturing treatments, smaller scale fracturing associated with these faults can be reactivated. This makes the formation of new induced fractures less likely.
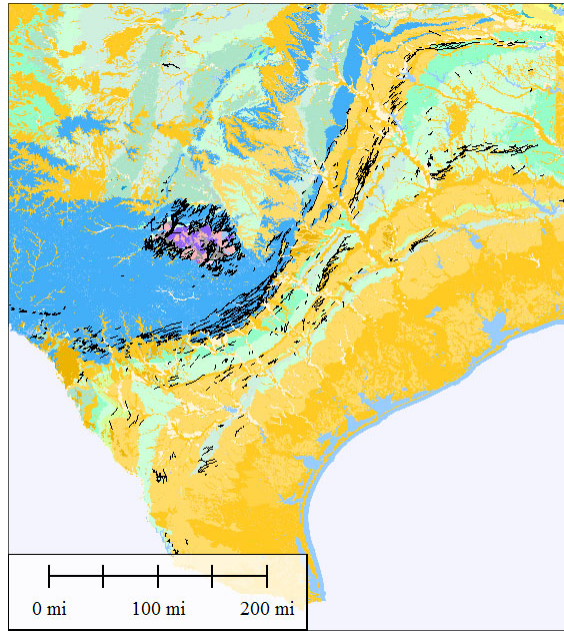
Figure 1. Map of the structural geology of southern Texas. Note the towards-the-gulf normal faulting striking NE-SW to ENE-WSW.

Hydraulic fracturing of pre-existing fractures is well documented in other unconventional reservoirs such as the Barnett Shale (Gale, 2007; Cipolla et al., 2008) and the Marcellus Shale (Williams-Stroud et al, 2012). Previous studies investigated source mechanism analyses of large amplitude events that corroborated complex failure behavior along pre-existing fracture networks in response to pressure changes induced by a hydraulic fracture treatment (Eisner et al., 2010; Wessels et al., 2011; Williams-Stroud et al., 2011).

The S_{Hmax} observed on the World Stress Map near the study area is ~N25E, about 20° off of the dominant trends in microseismicity. Figure 2 is a Digital Elevation Map of south Texas showing the surface lineaments. This relationship was also observed during the stimulation of a gas shale in the USA, where the dominant trends of microseismicity were controlled by pre-existing fractures and were non-parallel to SH_{max} (Williams-Stroud et al., 2012).

Methodology

Microseismic data were collected during the hydraulic fracture stimulation of three wells in the Eagle Ford Shale in south-central Texas. The array of geophones was laid out radially around the well pad and consisted of 1214 channels with 6 geophones per channel. Forty eight stages (16 per well) were hydraulically stimulated utilizing a perf and plug completion method, with a total of 96 hours of data recorded for the 3 wells. Microseismicity induced by the hydraulic fracture stimulation were imaged by a beamforming process, which is similar to a one-way depth migration. A velocity sub-volume was formulated, velocities were calibrated and perforation shots were used to validate the calibration.

More than 7000 microseismic events were located and thousands of these events displayed visible energy in the raw, unprocessed seismic traces. The remainder of the events were located utilizing the power of the stack, where the seismic amplitudes of all the traces across the array are summed. Figure 3 shows the final result of the processed microseismic events; note that two discrete trends are observed. Figure 4 is the final microseismic result in depth view, looking down the wellbore superimposed over a cross-section of the 3D volume. Events are colored by stage and sized by amplitude. The majority of the microseismicity displays long-linear trends at N40E and a less prevalent trend at N60E to N85E.
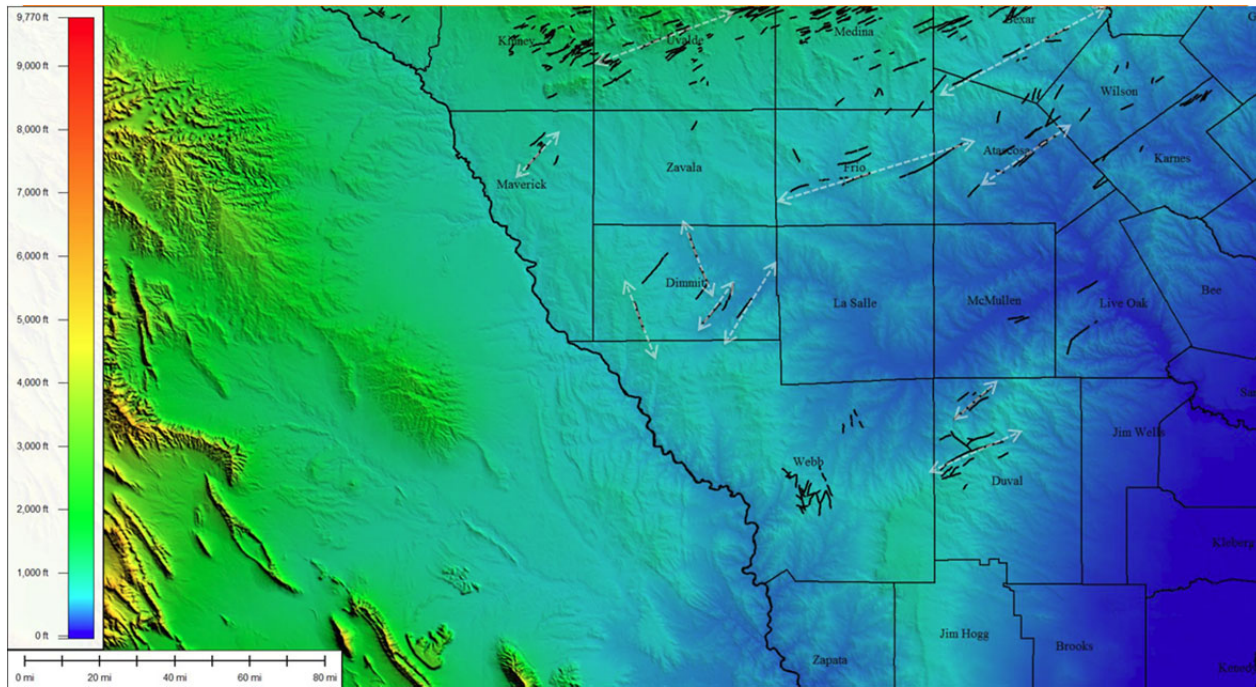
Figure 2. Digital Elevation Map of south Texas showing surface faults. Black lines mark the mapped lineaments and a selection of the faults have been labeled with white arrows. Note the dominant NE-SW and ENE-WSW trend of faulting.
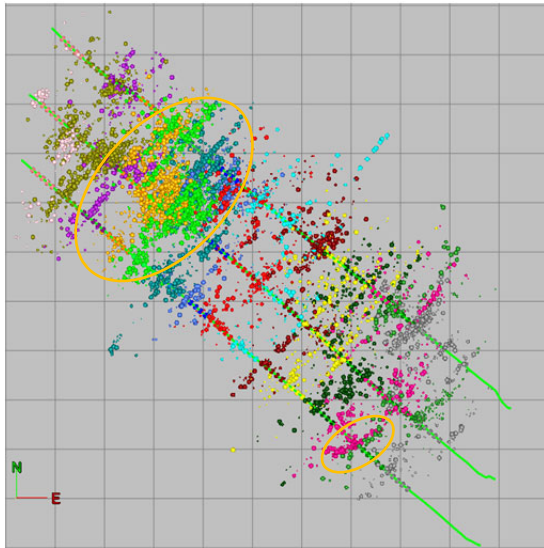

Figure 3. The final microseismic result for the 3 wells. Note predominant NE-SW trends in microseismicity and the ENE-WSW trend in the southwest stage (pink).
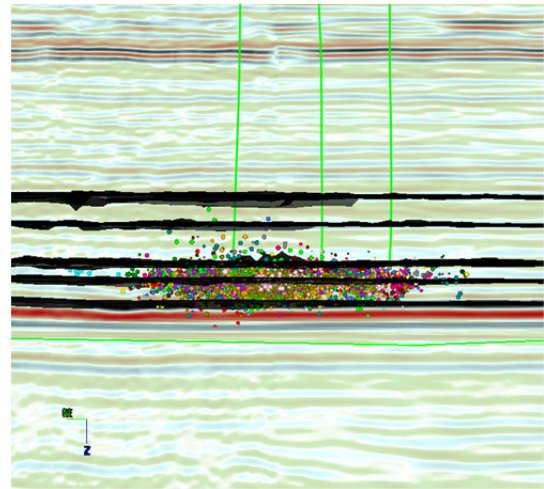

Figure 4. The final microseismic result in depth view looking down the wellbore superimposed over a cross-section of the 3D volume.

Determination of Subsurface Structure

Excellent signal strength and high amplitude microseismicity yields increased precision with respect to the event locations. For the 3H the average perforation error was 30' in X 28' in Y and 42' in the Z direction. These values are well within the size of the processing cells. With this type of accuracy comes great assurance in the event locations and therefore great assurance of the location of the fracture trends observed in the microseismicity. Data of this quality can be utilized to gain an understanding of the subsurface structure and to create subsurface fracture maps.

The major trends of microseismicity at N40E are parallel to the typical subsurface Gulf of Mexico growth faulting seen throughout Texas. These trends likely represent the reactivation of pre-existing regional joints or induced fractures. The minor trends at N60E to N85E are at an angle to S_{Hmax} and likely represent the reactivation of pre-existing faults (Figure 2). The microseismic event trends also parallel orientations calculated in source mechanism analyses, corroborating the source mechanisms and the trends in microseismicity. Figure 5 displays the source mechanism that is parallel to the dominant fracture trend, a high angle dip-slip fault striking to the NE-SW. Figure 6 displays the source mechanism of the secondary
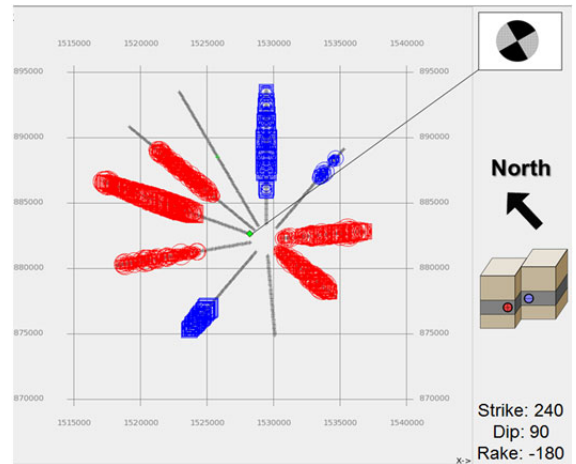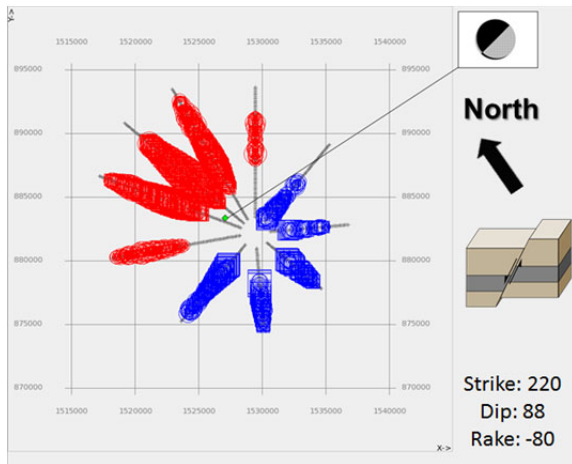
Figure 5 and Figure 6. The image on the left is the source mechanism for the NE-SW oriented failure plane and the image on the right is the ENE-WSW oriented failure plane. The red and white star represents the arms of the array. The circles represent the amplitude of the event and the squares represent the amplitude for the inversion. Where the color changes represents the nodal plane. The stereonet for each source mechanism is in the upper right hand corner and below that is a block diagram illustrating the type of slip on each plane. The strike, dip and rake for each mechanism is listed in the bottom right hand corner of the image.

set, a vertical strike-slip fault striking to the ENE-WSW. The relationship of induced fracture planes paralleling the source mechanism failure planes which are non-parallel to S_{Hmax} was observed in another US gas play (Wessels et al., 2011)

The observation of a higher frequency of microseismicity in long linear trends for the initial portion of the treatment (stages 3-6) followed by a lower frequency of microseismicity in stages 8-12, suggests that a large fault or group of fractures were opened during initial stages of the fracture treatment. The frac energy for the subsequent stages continued propagation into these fractures (Figure 7). The stages displaying a lower density of microseismicity suggest complex, induced fracturing due to a dearth of large, through-going, pre-existing fractures or reactivation of a complex, pre-existing network of fractures that allow the frac energy to be distributed more evenly. Figure 7 is the final data set superimposed over the seismic amplitudes across the Lower Eagle Ford Horizon. Note that the NE-SW trending long linear zones of microseismicity observed throughout the data set are congruent with the NE-SW trending seismic amplitudes.
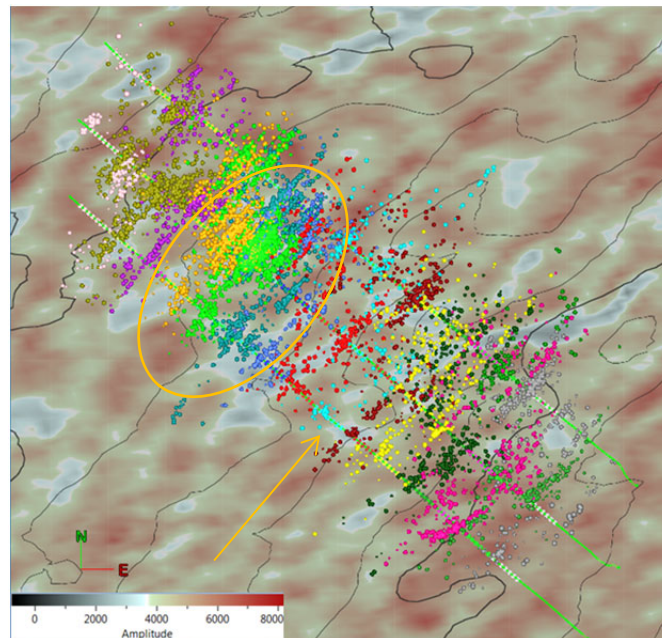

Figure 7. The final data set superimposed over the amplitudes across the Lower Eagle Ford Horizon. Also note the high event density in the northwest stages (green and yellow) highlighted by the orange ellipse, followed by diminished event density in the central portion of the data set, highlighted by orange arrow. Note the ENE-WSW trending amplitudes (light gray) which parallel the long linear trends of microseismicity observed throughout the data set.

Discrete Fracture Network (DFN) Modeling

The orientations of surface mapped faults and orientations of S_{Hmax} primarily derived from borehole breakout data as reported to the World Stress Map were used in conjunction with microseismicity trends observed to constrain the fracture orientations for the DFN. The N40E orientation was treated as the dominant orientation because the majority of the microseismicity trends formed in this orientation. This microseismicity is likely related to induced fracturing, reactivation of distributed fracturing around faults, or reactivation of a systematic joint set. The N20E, N60E, N85E, and N160E orientations are likely due to reactivation pre-existing faults. The N20E, N60E to N85E, and N160E orientations observed in microseismicity trends as well as in source mechanisms were less prevalent. The presence of these sets will likely make important contributions to the overall permeability. The four fracture sets for the DFN were generated as pseudo-deterministic fractures. This implies that the fractures were centered on the event locations and fracture sizes were based on the amplitude of the events. The assigned fracture size was 50-250 feet for all modeled fractures.

A geocellular model was generated for the events utilizing their locations and relative amplitudes as a fracture probability within the model. With such data sets containing high signal strength, a fracture is assigned to every event as opposed to a probabilistic approach where the probability of fracture generation at any location is related to the amplitude value in each cell. Figure 8 shows the DFN created from the geocellular model. The model displays all observed fracture sets, and presents a clear illustration of the geometry of the fracture network. The geocellular volume shows the distribution of the fracture permeability calculated from the fracture network. Note the higher permeabilities in the zones of dense microseismicity. The full permeability tensor is calculated from the total number of fractures in an individual grid cell, based on the fracture orientations and sizes. Figure 9 shows the geocelluar volume with relative permeability displayed.
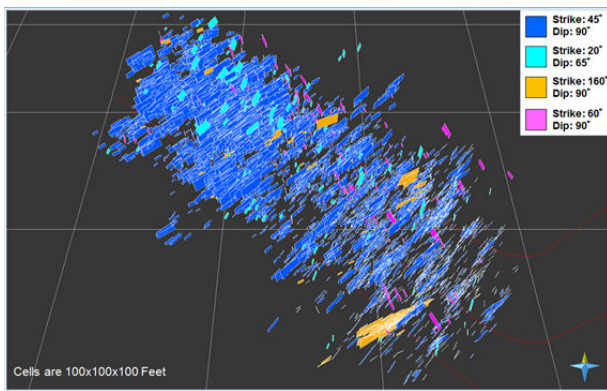

Figure 8. DFN created from the final microseismic events. Each fracture set is color coded. Note the higher density of fractures corresponding to the more dense zones of microseismicity.
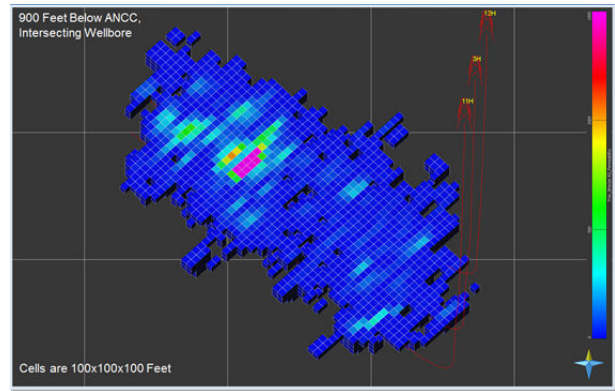

Figure 9. Geocelluar volume of stimulated permeability created using the DFN. Hot colors indicate high permeability. Dense zone of microseismicity correspond to highest permeability.

The flow properties obtained from the fracture models take into account the total sum of the areas of the fractures contained in each geocelluar grid. The fracture aperture is calculated proportionally to the fracture length, and the permeability tensor takes an average of all three of these attributes. Every cell containing a non-zero fracture flow property is included in the stimulated volume total. The volume of cells containing fracture flow properties is summed to obtain a total SRV for this treatment well. The total SRV volume is dependent on the size of the model cells and can be adjusted based on known reservoir flow properties. Only the portions of the modeled fractures within each cell are utilized to calculate the fracture porosity volume.

Conclusions

Utilizing a surface array, the full geometry of the microseismic result was viewed with no directional bias and the trends developed in the microseismicity pattern were representative of the true geometry of the subsurface fracture network. Source mechanisms were calculated for every event and were facilitated by the large aperture of the monitoring array, which also provided full coverage of the focal sphere of each source mechanism. The event source mechanisms showed different failure mechanisms and failure plane orientations in the fractures and faults.

The NE-SW trends observed in microseismicity and focal mechanisms correspond to induced fractures or reactivation of pre-existing regional joints. The ENE-WSW trends observed in microseismicity and focal mechanisms correspond to the reactivation of pre-existing faults. The dominant orientations of the fracture-related trends are parallel to extensional Gulf of

Mexico growth faulting and the faulting-related trends are at an angle of approximately 25° to the fracturing trends. These orientations are 15-45° from the current SH$_{max}$ in the region, validating the previous observation that fracturing during hydraulic fracture stimulations can induce new fracturing. However the fracturing is controlled by pre-existing fractures. Excellent signal strength and high amplitude microseismicity yields great assurance in the event locations and therefore great assurance of the locations of the fracture trends observed in the microseismicity. Microseismic data of this quality can be utilized to glean an understanding of the subsurface structure and to create subsurface fracture maps.

Acknowledgements

References

Cipolla, C.L., Warpinski, N.R., Mayerhofer, M.J. et al. 2008. The relationship between fracture complexity, reservoir properties, and fracture treatment design: *SPE Annual Technical Conference and Exhibition*, Denver, Colorado, USA. **SPE 115**.

Eisner, L., Williams-Stroud, S., Hill, A., Duncan, P., and Thornton, M. 2010. Beyond the Dots in the Box: microseismicity-constrained fracture models for reservoir simulations. *The Leading Edge*: 936-941.

Gale, J.F.W., Reed, R.M., and Holder, J. 2007. Natural fractures in the Barnett Shale and their importance for hydraulic fracture treatments. *AAPG Bulletin,* **v. 91**, i. 4: p. 603 - 622

Wessels, S., De La Pena, A., Kratz, M., Williams-Stroud, S., Jbeili, T. 2011. Identifying faults and fractures in unconventional reservoirs thorough microseismic monitoring. *First Break*, **v. 29(7)**: p. 99-1047.

Williams-Stroud, S., Barker, W.B., and Smith, K.L. 2011. Linear Bi-wing Fracture Trends Do Not Indicate Induced Hydraulic Fractures – The Rock Mechanics of Source Mechanisms. *EAGE*, 73rd EAGE Conference & Exhibition, Microseismic Methods.

Williams-Stroud, S., Barker, W.B., and Smith, K.L. 2012. Modeling the response of natural fracture networks to induced hydraulic fractures in stimulation treatments. EAGE First Break, **v. 30**: p. 71-75.

Williams-Stroud, S., Neuhaus, C. W., Telker, C, Remington, C., Barker, W., Neshyba, G., and Blair, K. 2012. Temporal evolution of stress states from hydraulic fracturing source mechanisms in the Marcellus Shale. Paper SPE 162786 presented at the 2012 SPE Canadian Unconventional Resources Conference, Calgary, Alberta, Canada, 30 Oct – 1 Nov.